Geomech. Geophys. Geo-energ. Geo-resour. (2022) 8:147
https://doi.org/10.1007/s40948-022-00455-6

ORIGINAL ARTICLE

Stability assessment of long gateroad pillar in ultra-thick coal seam: an extensive field and numerical study

Zhijie Zhu · Danqi Li

Received: 24 April 2022 / Accepted: 23 July 2022 / Published online: 26 August 2022

Abstract Sustainability of an underground longwall operation is highly dependent on stability of the pillars during the panels extractions to ensure the continuous serviceability of gateroads. In Chinese underground longwall mining, the gateroads are typically driven as a single roadway with a "long gateroad pillar" which is different to a common practice where a gateroad consists of a number of pillars known as chain pillars. Such a unique practice has been proven to be more economical with maximum recovery while the safety remains at its highest level. In this study, based on the data obtained from Tongxin coal mine in China, the mechanical stability of the driven long gateroad pillar was investigated. The focus was on two nearby longwall top coal caving panels and their impacts on the mechanical behaviour of long gateroad pillar during the longwall retreat. To do so, initially an area of the gateroad was selected for the field instrumentation and data collection. These included vertical stress measurement and depth of damage assessment within the gateroad pillar and the longwall panel. Hence, the convergence level of gateroad was quantified to be used for the numerical modelling and assessing the performance of the designed long gateroad pillar based on the finite difference modelling technique using FLAC^{3D}. Double-yield and strain-softening ubiquitous-joint constitutive models were used to simulate goaf material and strata, respectively. Finally, an extensive sensitivity analysis was conducted to compare the mechanical behaviour of a range of wide and narrow long gateroad pillars. It was concluded that the 50 m wide pillar is an ideal dimension for the future panels of Tongxin coal mine to achieve the maximum productivity and safety.

Article highlights

- The validated numerical model was used to study on stability of "long gateroad pillar".
- Premature yielding of the 38 m pillar would lead to severe geotechnical issues.
- Deep roof blasting of goaf edge or 50 m pillar can improve pillar conditions

Keywords Long gateroad pillar · Thick coal seam · Numerical model · Field measurement

Z. Zhu
School of Mining, Liaoning Technical University, Fuxin, China

Z. Zhu
State Key Laboratory of Coal Mining and Clean Utilization, Beijing, China

D. Li (✉)
WA School of Mines: Minerals. Energy and Chemical Engineering, Curtin University, Kalgoorlie, WA 6430, Australia
e-mail: danqi.li@curtin.edu.au

1 Introduction

There are many ultra-thick coal seams in China, such as in Datong, Changwu, Binchang and other mining areas with a large number of coal seams that are at least 8 m thick. Fully mechanized longwall top-coal caving in extra-thick coal seams typically produces large mining excavation spaces that lead to significant vertical displacements of strata. Complex and time delayed movements of goaf roof strata often occur due to very high roof collapse leading to stress redistribution that often causes difficult ground conditions (Zhu et al. 2018). During the mining process, the deformation and damage of the coal pillar and the adjacent roadway are extremely serious, which has a great impact on the safe and efficient production of the working face. In a typical underground longwall mining, a gateroad consists of two roadways being belt and travel roads which are separated through a number of pillars known as "chain pillars" (Whittaker and Singh 1981). However, in the Chinese underground longwall mining, a gateroad includes only a single roadway and the maingate and tailgate are separated through a long pillar known as "long gateroad pillar" without having the chain pillars or cut-throughs. Such a design has been proven to be efficient in many Chinese underground longwall operations. Also, it has been identified that the roof sagging, rib spalling or floor instability in the gateroads, potentially can be associated with the poor design of long gateroad pillar particularly when the width of pillar is small (Deng et al. 2019, Forbes et al. 2020, He et al. 2021a, b; Li et al. 2021a, b, Zhu et al. 2022). It is noteworthy that having a wide long gateroad pillar can lead to the loss of coal resources, thus, an efficient design of long gateroad pillar is critical to maintain the safety at the highest level while the maximum coal recovery can be achieved.

Salamon and Munro (1967) were the first who suggested an empirical formula to calculate the pillar strength in South African underground coal mines. Later, Bieniawski (1968) proposed an empirical relationship between the coal pillar strength and the sample size based on the field experiments performed on the large scale cubical shaped coal samples. Salamon (1970) identified the important factors that can contribute to the stability of pillars in deep underground coal mines. Hustrulid (1976) proposed two coal pillar strength models based on the pillar size and shape. Sheorey et al. (1981) considered the roof above the chain pillar as an elastic beam to assess the stability of pillar and the nearby gateroad. Barron (1984) developed a computer based analytical model that can determine the stability of coal pillar through brittle fracture or pseudo-ductile yield. Mark et al. (1995) introduced the analysis of retreat mining pillar stability (ARMPS) computer program which can be used in different mining methods. Galvin and Hebblewhite (1995) established the UNSW pillar design methodology as a useful tool for designing a square shaped coal pillar in Australian underground coal mining with high degree of certainty. Salamon et al. (1998) proposed a simple model for the pillar deterioration based on its size, to assess the long-term stability of coal pillar. Considering the abutment load due to the retreat mining and goaf, pillar stability assessment has been developed based on the tributary area theory and has been applied in the design of different pillars since 1967 (DP et al. 2002). Hill (2005) developed the pillar design criterion to protect the surface infrastructure based on a set of empirical equations. Ghasemi and Shahriar (2012) introduced the coal pillar design methodology through considering the abutment load to improve the safety of excavation in bord and pillar coal mines. Recio-Gordo and Jimenez (2012) defined a probabilistic prediction model for pillar stability based on ARMPS empirical method. Shaojie et al. (2016) developed a strip coal pillar design methodology based on an estimated surface subsidence in eastern China. Reed et al. (2017) assessed the suitability of coal pillar design criteria derived from the mechanistic interaction between the coal pillar and the overburden which was then followed by Prassetyo et al. (2019) who proposed a new coal pillar strength estimation formulae that includes the interface friction effect. (Vardar et al. 2019) firstly attempted to establish a numerical model to quantify the released energy during the failure of pillar-scale coal mass samples with varying cleat densities. The insights can aid in understanding the energy release mechanisms and associated coal burst potential in varying coal cleat conditions. (Sinha and Walton 2020) used the progressive S-shaped yield criterion to simulate the rib fracturing process in a longwall chain pillar at West Cliff mine and found damage was localized along the upper part of the pillar.

Stability of coal pillars can be affected by mining and geological factors such as pillar size, initial

stress, surrounding rock strength and mining method. Empirical and analytical methods for pillar design only include a limited number of parameters that can potentially lead to over-simplification (Sinha and Walton 2019). Current advancements in numerical modelling techniques have provided better opportunities for the detailed and fundamental understanding of pillar behaviour through including a large number of influencing factors under field setting. Mohan et al. (2001) used FLAC^{3D} numerical modelling to evaluate the pillar strength based on the practical cases from India. Jaiswal and Shrivastva (2009) established a numerical model to investigate the strain-softening behaviour of a number of coal pillars along with the assessment of some failed and stable cases. Li et al. (2014) established two longwall models to back-analyse the stability of different pillars leading to a physical based methodology for the efficient pillar design. Das et al. (2019) simulated the stress and failure characteristics of inclined coal pillars and concluded that the pillar strength decreases with an increase in the coal seam dip. Further studies based on the numerical modelling for stability assessment of coal pillars and gateroads were conducted by other researchers (Bai et al. 2017; Jiang et al. 2017; Zhang et al. 2017; Wu et al. 2018).

While a large number of studies have been conducted on the pillar design from empirical, analytical and numerical studies, yet no study has investigated the stability of "long gateroad pillar" in the thick coal seam which is a common practice in Chinese underground longwall mining. Due to the presence of such a thick coal seam, often the underground coal mining in China is combined with the coal caving system resulting in longwall top coal caving (LTCC) mining. Such an advanced LTCC operation with a single "long gateroad pillar" can potentially be problematic if the pillars dimensions, particularly the width are not well characterised. Thus, in here, it is aimed to investigate the mechanical behaviour of such a long pillar during the LTCC mining in Tongxin coal mine. The mine is currently operating in 15 m extra-thick coal seam under competent and strong sandstone roof. The instability of gateroad pillars has adversely affected the safe and sustainable production. Based on an extensive literature review, it has been noted that very little or indeed no study has included such a complex pillar stability problem and indeed, this work will be the first of its kind to tackle this problem. An extensive field investigation was conducted including the roadway convergence monitoring, stress measurement and pillar stress variation monitoring to analyse the roadway deformation and the stability of long gateroad pillar. Finally, the finite difference model (FLAC^{3D}) was used to conduct the parametric study on the long gateroad pillar in Tongxin mine followed by establishing a suitable guideline for the long gateroad pillar design which can potentially serve as a suitable benchmark for any future mining operations under similar conditions.

2 Mine layouts and geological conditions

Tongxin coal mine is located in the Datong coalfield in Shanxi province, China (see Fig. 1a). The thickness of coal seam is about 15 m dipping from 1 to 4 degrees at the depth of 450 m below the surface. The lithology of coal strata is listed in Table 1 and the mechanical properties of coal measure rocks at about 3 to 5 m above the coal seam is given in Table 2. The LTCC method has been employed in which, the 3.9 m of coal seam is extracted from the longwall panels and up to about 11 m through the caving. The focus of this study is on panels8103 and 8104. The length and width of panel8103 were 1932 m and 200 m, respectively. The width of panel8104 was the same as panel8103 while its length was slightly longer at 1950 m. Maingate and tailgate were driven with a single roadway as shown in Fig. 1. It is noteworthy that due to the poor design of long gateroad pillar which led to this study, panel8104 was extracted first followed by panel8103. The width of roadways was 5.3 m and its height was consistent with the height of coal extraction at 3.9 m. Rock bolts, point anchor cables, steel mesh and steel beams were the typical support systems used in the gateroads (see Fig. 2 and Table 3).

3 Field study

3.1 Instrumentation

A measurement station was set up at the tailgate of panel8103 located 800 m far from the longwall install face (see Fig. 1). Hydraulic stress cell was utilized to monitor the vertical stress. Six stress cells were

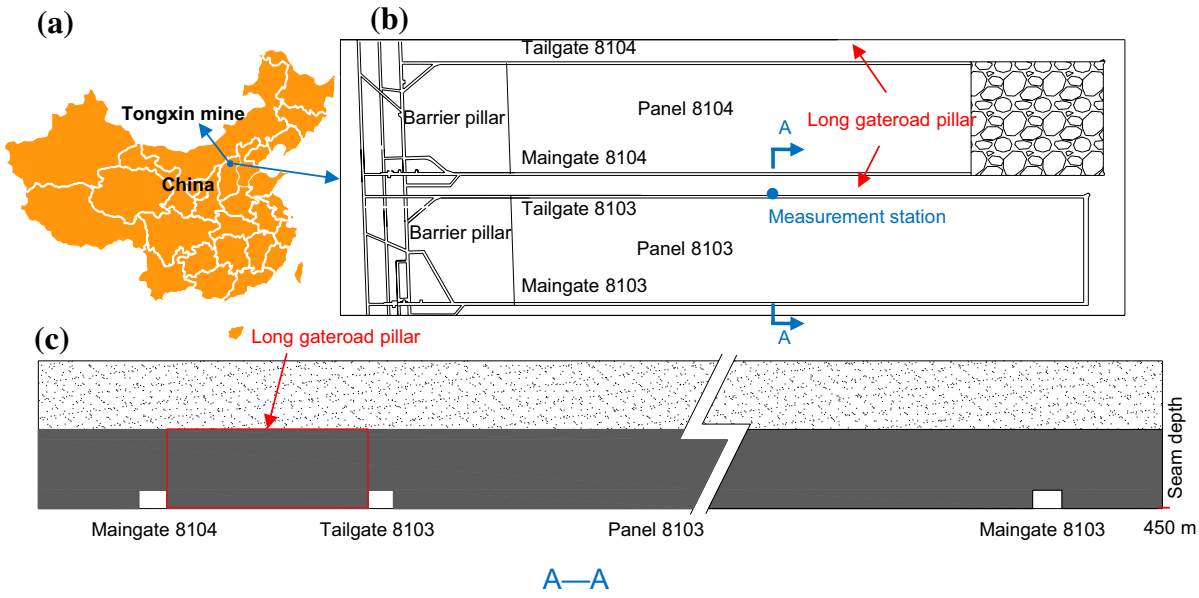

Fig. 1 Tongxin coal mine including: **a** the location of mine, **b** plan view of panels8103 and 8104 and **c** cross-section of roadways layout

installed inside the interested long gateroad pillar between the maingate8104 and tailgate8103 in addition to three cells in the block side as demonstrated in Fig. 3. Also, the vertical and horizontal convergences were measured using the laser rangefinder. All the instrumentations were installed before the commencement of coal extraction in panel8104. The monitoring was carried out at two stages: (I) extraction of panel8104 and (II) extraction of panel8103. The collected data during the two stages were used to investigate how the progress of longwall operation can impact on the stability of long gateroad pillar and the surrounding areas. It is noteworthy that during the stage II, when the longwall face approached the measurement station, most of the monitoring equipment were destroyed except the convergence measurement devices.

3.2 Stress distribution profile in the long gateroad pillar

During the retreat of panel8104, the change in the vertical stress was measured using the monitoring cell and the resulting stress profiles are shown in Fig. 4. When the longwall face was 20 m ahead of the measurement station, the peak vertical stress on the long gateroad pillar increased to about 15 MPa. When the longwall face was adjacent to the measurement station, the peak stress increased to approximately 17.5 MPa and then dropped to 7.5 MPa when the longwall was 50 m beyond the measurement station. This can potentially indicate the yielding of the long gateroad pillar at about 8 m into the pillar from the rib of maingate8104. When the longwall face passed 100 m of the measurement station, the peak vertical stress of 22 MPa was measured at about 23 m into the pillar from the rib of maingate8104. The stress cell located 13 m far from the maingate8104, dropped to 11.5 MPa indicating the potential yielding of pillar at that location. When the longwall was at 300 m beyond the measurement station, the vertical stress of about 25 MPa was recorded at 28 m distance from the rib of maingate8104 into the pillar (see Fig. 4).

After complete excavation of panel8104, two horizontal boreholes with 10 m length and 40 mm diameter were drilled into the pillar and coal block (panel8103) in tailgate8103 as shown in Fig. 5. The damage in the boreholes was assessed through borescope and noted that the majority of cracks occurred at 4.8 m and 7.5 m into the boreholes from the collars.

Table 1 Lithology of section A–A shown in Fig. 1

Layer number	Lithology	Thickness (m)	Depth (m)	Layer number	Lithology	Thickness (m)	Depth (m)
1	Sandy mudstone	3.2	290.7	20	Coarse sandstone	13	389.8
2	Coarse sandstone	8.2	293.9	21	Fine-grained sandstone	1.1	402.8
3	Coal	4.0	302.1	22	Coarse sandstone	7.9	403.9
4	Fine-grained sandstone	6.5	306.1	23	Fine-grained sandstone	3.0	411.8
5	Coarse sandstone	7.5	312.6	24	Coarse sandstone	2.1	414.8
6	Siltstone	3.8	320.1	25	Sandy mudstone	1.0	416.9
7	Fine-grained sandstone	3.7	323.9	26	Coarse sandstone	5.1	417.9
8	Siltstone	3.9	327.6	27	Fine-grained sandstone	3.6	423
9	Fine-grained sandstone	3.1	331.5	28	Siltstone	2.6	426.6
10	Siltstone	7.7	334.6	29	Coarse sandstone	2.3	429.2
11	Coarse sandstone	2.1	342.3	30	Fine-grained sandstone	4.1	431.5
12	Siltstone	11.4	344.4	31	Siltstone	3.8	435.6
13	Fine-grained sandstone	3.5	355.8	32	Fine-grained sandstone	1.2	439.4
14	Coarse sandstone	6.3	359.3	33	Coarse sandstone	9.4	440.6
15	Sandy mudstone	12.8	365.6	34	3–5 coal	15	450
16	Fine-grained sandstone	1.8	378.4	35	Sandy mudstone	1.9	451.9
17	Siltstone	4.1	380.2	36	Coarse sandstone	3.1	455
18	Fine-grained sandstone	1.9	384.3	37	Siltstone	4.4	459.4
19	Sandy mudstone	3.6	386.2	38	Fine-grained sandstone	4.5	463.9

Table 2 Intact rocks and joints parameters measured from the laboratory experiments

Rock Type	Intact rock							Joint	
	Density (kg/m^3)	Young's modulus (GPa)	Poisson's ratio	Cohesion (MPa)	Friction angle (°)	Uniaxial compressive strength (MPa)	Tensile strength (MPa)	Cohesion (MPa)	Friction angle (°)
Fine sandstone	2560	27.8	0.21	27.2	39.1	117.2	18.4	3.7	17.2
Coarse sandstone	2383	16.1	0.17	17.2	40.7	73.2	12.4	2.4	19.5
Siltstone	2532	24.9	0.24	20.6	39.6	86	15.4	2.9	17.7
Sandy mudstone	2570	18.9	0.22	12.6	36.3	49.6	8.8	1.4	18.6
Coal	1373	3.9	0.30	4.1	29.9	14	1.65	0.6	10.6

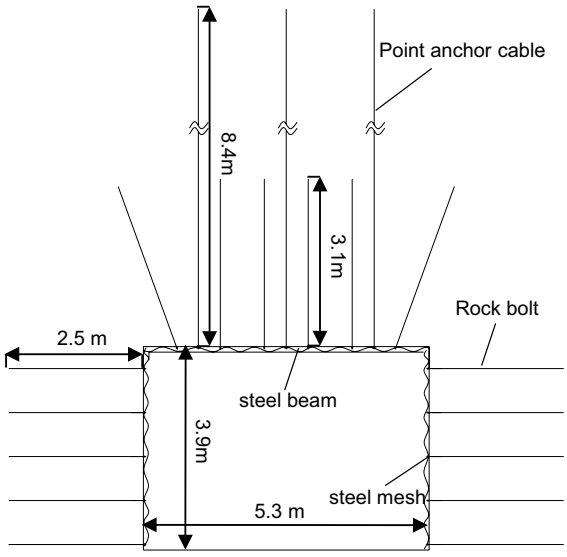

Fig. 2 Examples of the typical support systems in a gateroad

3.3 Roadway convergence measurement

The convergence changes at the measurement station are shown in Fig. 6. The convergence under both vertical and horizontal directions found to be similar during the single sided goaf loading (stage I). The convergence began to change 100 m ahead of the longwall face and then stabilized approximately 200 m beyond the face. At 400 m beyond the face, the horizontal and vertical convergence measurements were 205 mm and 340 mm, respectively (see Fig. 6a). Under the influence of double sided goaf loading (stage II), the convergence began to increase when the panel8103 was 120 m ahead of the measurement station (Fig. 6b). The tailgate began to severely deform as the face approached the measurement station. The maximum measured horizontal and vertical convergence was 1956 mm and 2074 mm, respectively at the measurement station during the double sided goaf loading.

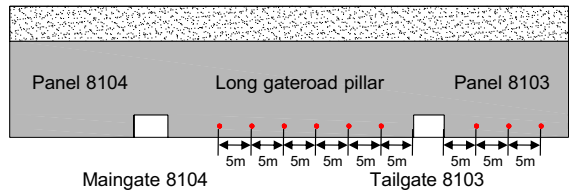

Fig. 3 Instrumented site showing the location of hydraulic stress cells

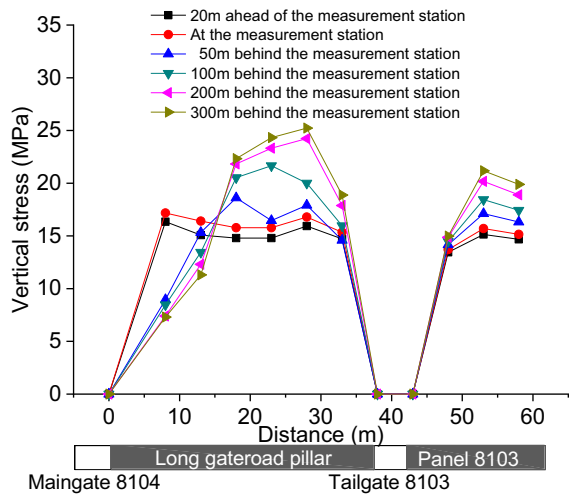

Fig. 4 Long gateroad pillar stress profiles due to retreat of panel8104

4 Numerical modelling

4.1 Model parameters estimation

Estimating the proper input parameters for the numerical modelling is essential, particularly when the rock properties are upscaled from the laboratory size to the field setting (Coggan et al. 2012, Masoumi et al. 2014, 2016, 2017, 2018; Zhai et al. 2020). For the upscaling process, the resulting

Table 3 Detailed information of the typical support systems in the gateroads

Type	Length (mm)	Hole diameter (mm)	Interval (mm)	Row spacing (mm)
Rib bolt (point anchor)	2500	18	800	800
Roof bolt (point anchor)	3100	20	800	800
Roof cable (point anchor)	8400	22	1600	1600

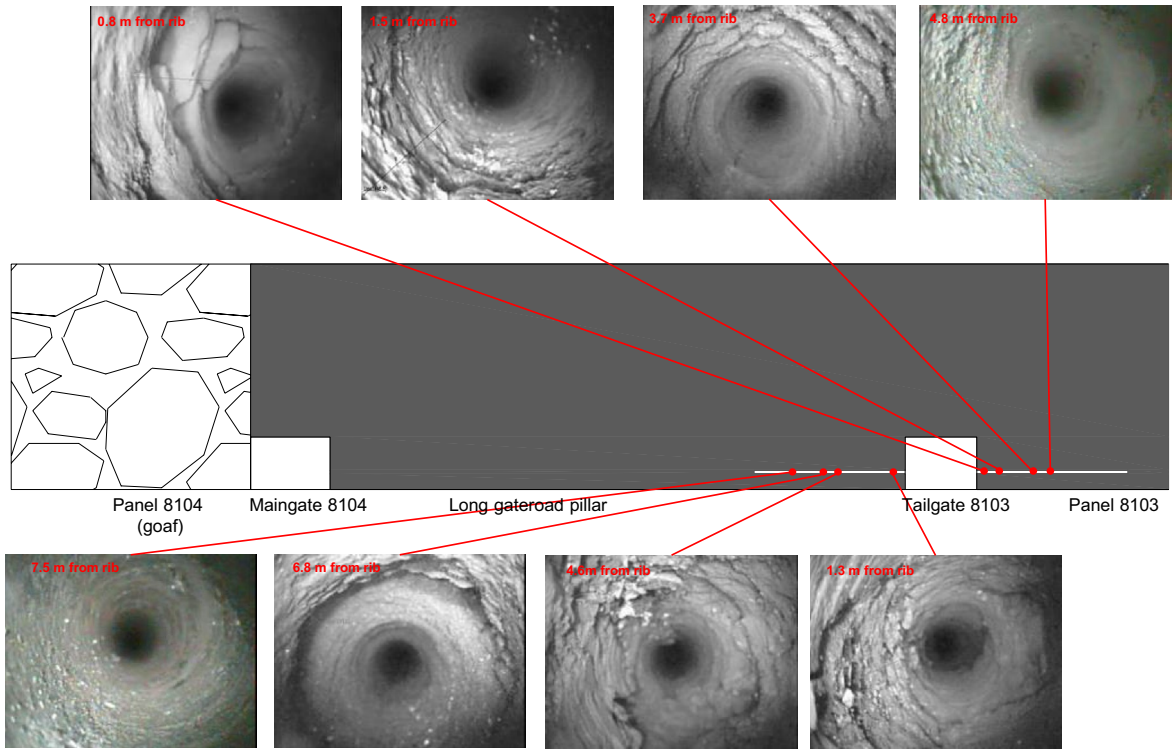

Fig. 5 Borescope images obtained from two holes in rips of tailgate8103 after complete retreat of panel8104

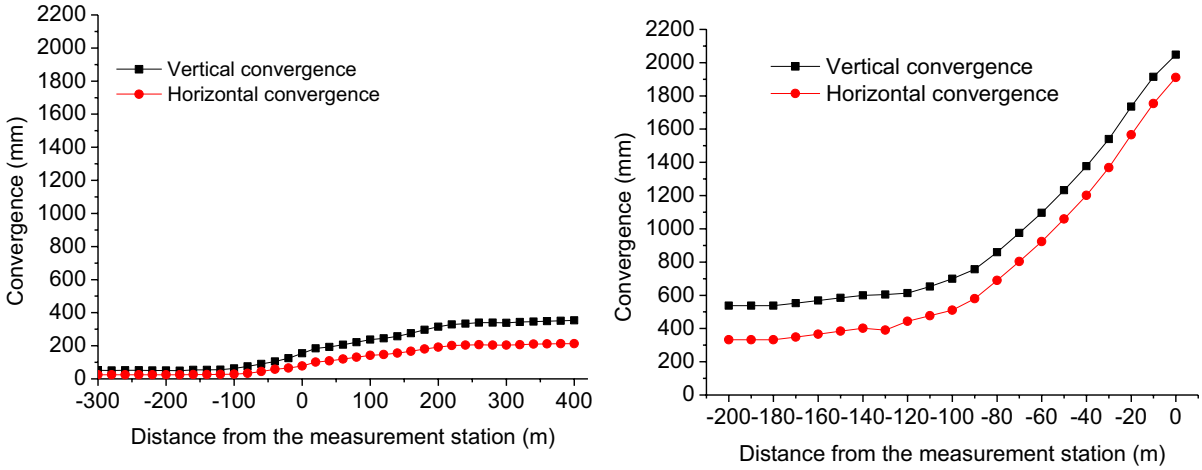

(a) Stage I **(b)** Stage II

Fig. 6 Induced convergence changes due to the extraction of panels **a** Stage I and **b** Stage II

coal strength properties from the laboratory environment can be adjusted using the reduction factors suggested by Wilson (1983) based on United Kingdom coal mining guidelines. Wilson (1983) introduced a set of conditions for upscaling the uniaxial compressive strength from the laboratory size to the field setting as follows:

$$\sigma_{in-situ} = \sigma_{lab}/f \quad (1)$$

where f can be determined from Table 4.

According to the core logging data obtained from Tongxin mine, the joints were scarce in the roof of roadways (see Fig. 7), thus, the f value of 2 was chosen in such a roof condition. Also, due to the distinctly cleated structure of coal with intermittent bright and dull layers, its f value was estimated at 5.

In rock engineering, RQD, RMR and GSI are commonly used for rock mass classification (Mo et al. 2020). Zhang and Einstein (2004) determined the relationship between RQD and the ratio between the elastic modulus of rock mass and rock sample according to:

$$\frac{E_m}{E_r} = 10^{0.0186RQD-1.91} \quad (2)$$

where E_m is the elastic modulus of rock mass and E_r is the elastic modulus of rock sample. In this study, the mean RQD values for rock strata and coal seam were estimated at 88 and 72, respectively.

In a summary, the strength parameters for rock mass including the compressive and tensile strengths as well as cohesion can be determined through upscaling from intact rock testing results (see Table 2) according to Eq. (1). Rock mass elastic modulus can be determined through empirical equation according to Eq. (2). The friction angles for rock mass were assumed to be the same to those for intact rock and joint obtained through rock testing. The dilation angle for coal was found to be 2° while for the rock strata it was estimated at 5° according to Singh GSP and Singh UK (Singh and Singh 2009). The strength parameters for bedding were determined based on the direct shear testing results (see Table 2). The cohesions of beddings are determined by upscaling the results of cohesion for joints according to Eq. (1) whereas the friction angles of beddings were assumed to be the same to those for joints. As such, all the mechanical parameters for the numerical model are shown in Table 5.

For coal seam and rock strata, the joints or cleats can dominate their mechanical behaviour (Lorig and Cabrera 2013; Das et al. 2017). Thus, the application of strain-softening ubiquitous-joint constitutive model in FLAC^{3D} found to be a suitable technique which is routinely utilized to model the laminated/bedded/jointed materials that exhibit non-linear

Table 4 Conditions for upscaling the strength of coal from the laboratory size to the field setting (after Wilson 1983)

f	1	2	3	4	5	6 or 7
Rock mass condition	Massive unjointed rock	Widely spaced joints	More jointed but still massive	Well-jointed and weaker rock	Closely cleated rock such as coal	Weak rock in neighbourhood of fault plane

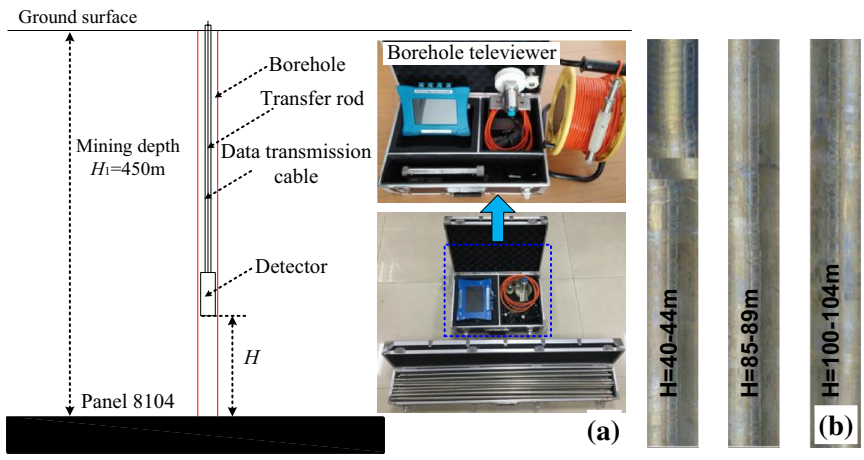

Fig. 7 Core logging equipment including: (**a**) borehole televiewer survey (**b**) and the resulting borehole images

Table 5 Rock and joint mechanical parameters used in the numerical models

Rock Type	Rock mass								Bedding plane	
	Density (kg/m^3)	Young's modulus, (GPa)	Poisson's ratio	Cohesion (MPa)	Friction angle (°)	Dilation angle (°)	Uniaxial compressive strength (MPa)	Tensile strength (MPa)	Cohesion (MPa)	Friction angle (°)
Fine sandstone	2560	14.8	0.21	13.6	39.1	5	58.6	9.2	1.8	17.2
Coarse sandstone	2383	8.6	0.17	8.6	40.7	5	36.6	6.2	1.2	19.5
Siltstone	2532	13.3	0.24	10.4	39.6	5	43	7.7	1.5	17.7
Sandy mudstone	2570	10.1	0.22	6.4	36.3	5	24.8	4.4	0.7	18.6
Coal	1373	0.8	0.30	0.8	29.9	2	2.8	0.33	0.1	10.6

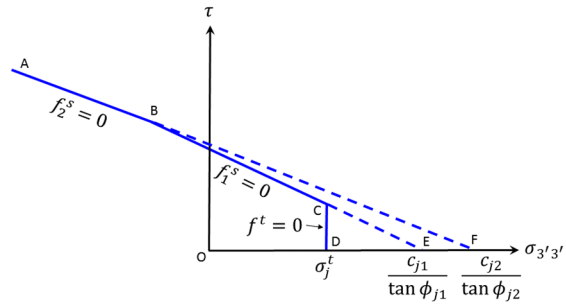

Fig. 8 Bilinear joint failure criterion in strain-softening ubiquitous-joint constitutive model.[52]

softening behaviour. The previous numerical works have illustrated that such a method is reliable enough to simulate the failure and deformation behaviour of layered strata (Sainsbury et al. 2008, Sainsbury and Sainsbury 2017, Hu et al. 2019).

The joint properties were used in the numerical model. The stresses, corrected for plastic flow in rock, are transformed into two components being parallel and perpendicular to the joint plane and tested for failure. The tangential and normal movement magnitudes determine the joint failure expressed by: $\tau = \sqrt{\sigma_{1`3`}^2 + \sigma_{2`3`}^2}$ (The local axis 1`is in the dip direction, 2` the strike, and 3` the normal to the weak plane.).

The rock joint failure is shown in Fig. 8 including two Mohr–Coulomb failure criteria ($f_2^s = 0$ in zone A-B, and $f_1^s = 0$ for zone B-C) and a tension rock failure ($f^t = 0$ for zone C-D). The shear failure represented by $f^s = 0$ using a cohesion (c_j) and an angle of friction ($\varnothing_j$) with c_{j_2}, $\varnothing_{j_2}$ in zone A-B, and c_{j_1}, $\varnothing_{j_1}$ in zone B-C. The tension is described by the tensile strength of rock (σ_j^t). Therefore:

$$f^s = \tau + \sigma_{3`3`} \tan \emptyset_j - c_j \tag{3}$$

$$f^t = \sigma_{3`3`} - \sigma_j^t \tag{4}$$

The softening behavior of rock and rock joints are given in terms of four softening rock properties that determine the shear and tensile strains. In the bilinear strain-softening ubiquitous-joint model, the yielding parameters such as cohesion, angle of

friction, dilation and tensile strength for rock and rock joints are calculated automatically (Itasca 2011).

The stain softening ubiquitous-joint parameters of different strata layers need to be calibrated before the simulation. Therefore, the calibration models were established to simulate the uniaxial compressive and Brazilian tensile testing on the samples. For the uniaxial compressive test, the length to dimeter ratio was 2 and the diameter was 2 m. For the Brazilian modelling, the same diameter as that for the uniaxial compressive loading was used but the length to diameter ratio was 0.5. Figure 9 demonstrates the modelling process under uniaxial compressive and Brazilian testing conditions. The resulting mechanical parameters for five different rock types are presented in Table 6.

4.2 Double-yield constitutive model for goaf simulation

A set of analytical models proposed by Salamon (1990) is widely used to quantify the mechanical properties of goaf as follows:

$$\sigma = \frac{E_0 \varepsilon}{1 - \varepsilon/\varepsilon_m} \tag{5}$$

$$\varepsilon_m = \frac{b - 1}{b} \tag{6}$$

$$b = \frac{h_{cav} + h_m}{h_{cav}} \tag{7}$$

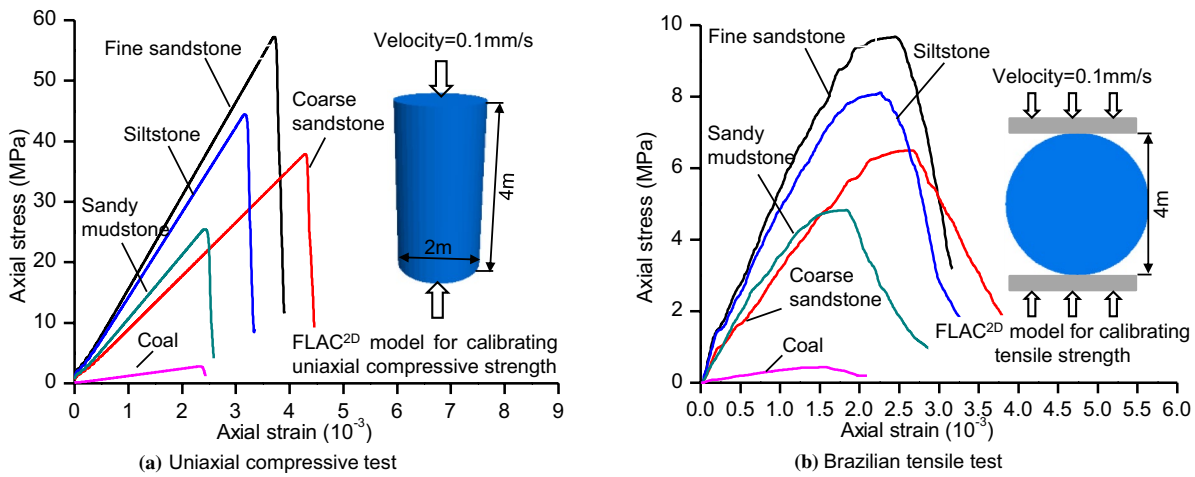

Fig. 9 Calibrated parameters for **a** uniaxial compressive and **b** Brazilian tensile tests

Table 6 The resulting mechanical parameters for five different rock types obtained from the numerical simulations

Rock Type	Young's modulus (GPa)			Uniaxial compressive strength (MPa)			Tensile strength (MPa)		
	Rock mass	Numerical	Difference (%)	Rock mass	Numerical	Difference (%)	Rock mass	Numerical	Difference (%)
Fine sandstone	14.8	15.2	2.7	58.6	57.8	1.4	9.2	9.7	5.4
Coarse sandstone	8.6	8.9	3.5	36.6	38.2	4.4	6.2	6.5	4.8
Siltstone	13.3	13.9	4.5	43	45	4.6	7.7	8.1	5.2
Sandy mudstone	10.1	10.7	5.9	24.8	25.8	4.0	4.4	4.7	6.8
Coal	0.8	0.83	3.8	2.8	2.9	3.6	0.33	0.31	6.1

$$E_0 = \frac{10.39\sigma_c^{1.042}}{b^{7.7}} \quad (8)$$

where ε_m is the maximum strain of goaf material, E_0 is the initial goaf modulus, b is the bulking factor, h_m is the mining height, h_{cav} is the height of caved zone and σ_c is the in-situ vertical stress. The height of caved zone was estimated at 80 m according to the field data obtained from EH4 electromagnetic image system (Wu et al. 2019) for mining height of 15 m. The maximum strain and bulking factor of goaf were estimated from Eqs. (6) and (7) at 0.15 and 1.16, respectively. The in-situ vertical stress (σ_c) in the same coal strata was reported 11.3 MPa by Chen et al. (2016). As a result, the Salamon (1990) stress–strain relationship (Eq. 5) was used to quantify the goaf movement for comparison with the numerical results. Table 7 shows a number of estimated stresses by the changes in strain according to Salamon (1990) stress–strain relationship.

Double-yield constitutive model in FLAC^{3D} was used to simulate the goaf behaviour and then the results were compared with those obtained from Salamon (1990) model for verification purposes. The mechanical parameters for double-yield constitutive model are listed in Table 8. In such a constitutive model, a number of mechanical parameters such as bulk and shear moduli as well as cohesion and friction angle are required. It is noteworthy that the bulk and shear moduli can be estimated through the trial and error process. A single-cube element (1 m × 1 m × 1 m) was modelled by FLAC^{3D} and the resulting stress–strain curve was compared to that obtained from Salamon (1990) model as shown in Fig. 10. Noticeably, two graphs match very well confirming the suitability of double-yield constitutive model in FLAC^{3D} for goaf simulation.

Table 7 Stress–strain estimation in goaf according to Salamon [53] analytical model

Strain	Stress (MPa)
0	0
0.01	0.66
0.02	1.41
0.03	2.28
0.04	3.3
0.05	4.5
0.06	5.96
0.07	7.74
0.08	9.98
0.09	12.9
0.10	16.8
0.11	22.3
0.12	30.8
0.13	45.3
0.14	76
0.15	185

Table 8 Mechanical parameters for goaf material

Bulk modulus (GPa)	Shear modulus (GPa)	Density (kg/m^3)	Cohesion (MPa)	Friction angle (°)	Dilation angle (°)
8.6	6.3	2000	0.1	5	6

4.3 Model construction and simulation

Longwall panels8103 and 8104 were simulated for the numerical modelling as shown in Fig. 11. The dimension of the model is 538 m × 400 m × 200 m. For computational efficiency, the concentration of meshing was on the coal seam and goaf area at about 300 m below the surface and its corresponding vertical stress. The typical caving angle for weak strata is between 65 and 80° and for strong strata it ranges from 55° to 65° according to Galvin (2016). In here, the caving angle of 55° was used according

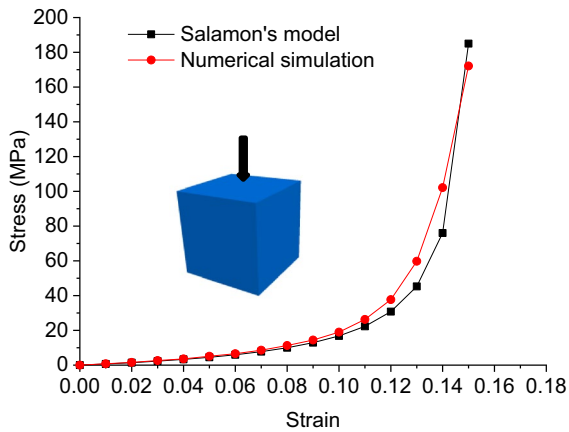

Fig. 10 Comparison between the analytical and numerical simulations

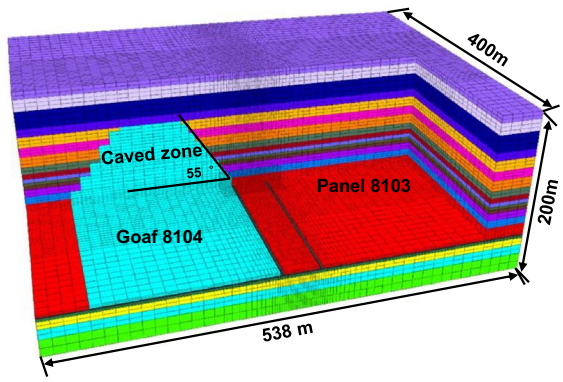

Fig. 11 Numerical model geometry

to the field data. Double-yield constitutive model in FLAC^{3D} was used to simulate the goaf behaviour where the strain-softening ubiquitous-joint constitutive model was used to simulate the pillar material and strata. Pillar yielding can be examined by the plastic zone state.

Considering the field condition, the horizontal displacements were fixed at the lateral boundaries while the vertical displacements were only fixed at the bottom boundary. The in-situ vertical stress of 13.8 MPa, maximum and minimum horizontal stresses of 19.6 MPa and 11.6 MPa, respectively were measured at the depth of 470 m below the surface using the borehole stress relief method (Chen et al. 2016). The longwall advance direction was measured to be parallel to the maximum principal stresses. Hence, the initial stress of this model in X and Y-directions were calculated to be from 7.4 MPa to 12.3 MPa and 12.5 MPa to 20.9 MPa, respectively. As the lateral boundaries were constrained, the stress was initiated in the zones of different layers before excavation. The applied vertical stress on the top boundary was 8.8 MPa.

The longwall retreat was parallel to the maximum horizontal stress. The simulation steps consisted of (a) excavation of tailgate 8103 and maingate 8104; (b) retreat of panel 8104 and finally, (c) retreat of panel 8103. In each step, the excavated coal and the caved zone were replaced by the double-yield goaf material.

4.4 Validation of the modelling

In order to demonstrate the validity of the modelling works, the simulation of the instrumented section (station) in tailgate8103 which was explained earlier (see Fig. 1) was compared with the field observations. Figure 12 illustrates the convergence of roadway in tailgate8103 after complete retreat of panel8104 exhibiting floor heaving, roof sagging and rib sloughing. All these three behaviours have been well simulated by the numerical model confirming the validity

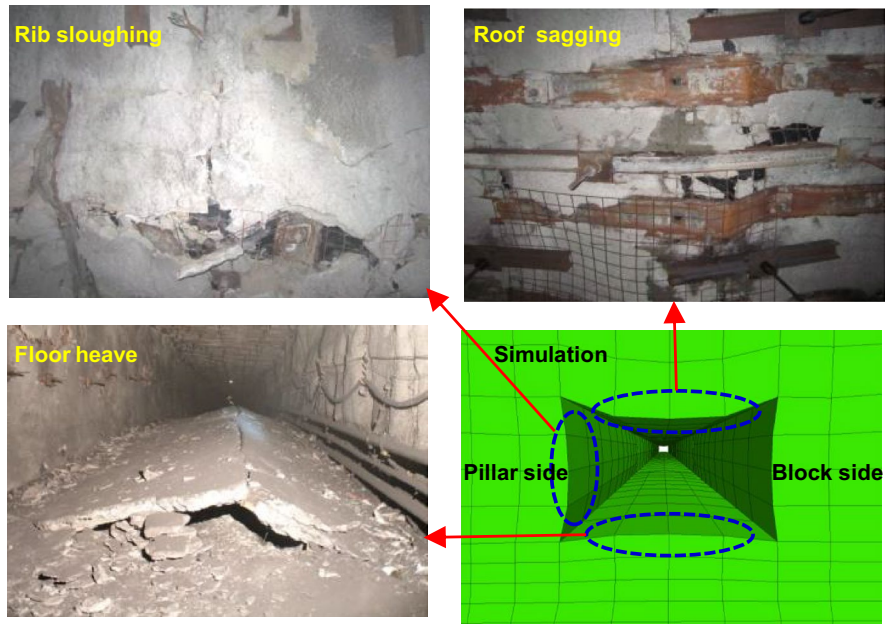

Fig. 12 Comparison between the field observations and the numerical model in tailgate8103

of the modelling procedure. In addition, the measured horizontal and vertical convergences at the instrumented site (see Fig. 6), as well as the failure depth of ribs were compared with the estimated convergences and ribs failure depths by the numerical models in Table 9 indicating a good agreement between the field measurements and the numerical results.

4.5 Stability assessment of long gateroad pillar

From the field stress measurement (see Fig. 4), the critical role of long gateroad pillar in controlling the stability of gateroads has been well appreciated particularly in an underground longwall mining with strong roof. On the other hand, it is clear that with the progress of mining operation, the gradual increase in goaf areas can induce additional stress (or so-called stress concentration) on the long gateroad pillar. Thus, it is required to assess the stability of long gateroad pillar under various stress conditions associated with the panels retreat through a set of numerical simulations. This can be divided into two stages including the retreat of panels I) 8104 and II) 8103, respectively. Simulation results of the long gateroad pillar during the retreat of panels8104 (stage I) and 8103 are shown in Fig. 13 and Table 10.

During the retreat of panel8104 (stage I), the increase in the vertical stress on the long gateroad pillar commenced when the panel was approximately 100 m ahead of the measurement station (see Fig. 1). Therefore, through the numerical results, it is predicted that by the time that the panel reaches to the measurement station, the long gateroad pillar stress profile forms a saddle shape in which the vertical stress is estimated to be 20 MPa and 17.4 MPa at 9 m and 33 m far from panel8104, respectively (see Fig. 13a). Also, when panel8104 is at the measurement station, it is estimated that the vertical stress on the block side of tailgate8103 increases to about 15.6 MPa. With the advancement of panel 8104, additional vertical stress is applied on the pillar sides leading to the yielding of long gateroad pillar as shown in Fig. 13b–d. The progress of yielding on the sides of gateroad pillar can result in the concentration of vertical stress on the centre point of pillar which is partially yielded and consequently can lead to pillar failure if the strength of pillar lies lower than the concentrated vertical stress. Figure 12 demonstrates the effects of these stress changes on long gateraod pillar where the tailgate8103 has been severely converged with significant roof sagging and floor heaving.

During the retreat of panel8103 (stage II), the pillar vertical stress profile follows the unimodal shape (Fig. 13e–h). When panel8103 was 100 m ahead of the measurement station, the numerical results predicted the maximum vertical stress of 36.6 MPa at about 10 m far from the rib of tailgate8103. Such a prediction was consistent with what was observed and reported from the field work indicating a severe deformation in tailgate8103 when panel8103 was about 100 m to 120 m ahead of the measurement station. When the panel was 50 m ahead of the measurement station, the complete pillar failure was predicted. At this point, the vertical stress at the centre of pillar decreased slightly to 36 MPa while it increased to about 39.4 MPa on the block side of panel8103 (see Fig. 13f). When the panel was at 10 m ahead of measurement station, the vertical stress on the pillar was predicted to decrease further to about 27.8 MPa and the stress on the block side was also expected to reduce at about 14 MPa while the yielding in the rib zone of tailgate8103 was expanding.

Table 9 Comparing the measured convergences and rib failure depths with the numerical results in tailgate8103

	Field measurement	Simulation
Horizontal convergence (mm)	205	180
Vertical convergence (mm)	340	320
Failure depth of pillar rib (m)	7.5	8
Failure depth of solid rib (m)	4.8	5

4.6 Sensitivity evaluation of the narrow and wide long gateroad pillars

From the earlier section, the critical role of long gateroad pillar has been highlighted where any under-designing can lead to significant gateroad convergence or even failure at longwall face due to stress concertation associated with rib abutment or severe stress notching issue (Zhang et al. 2016; Peng 2019). On the other hand, the over-designing can reduce the recovery of coal production which is not desirable. Therefore, a sensitivity analysis on the behaviour of long gateroad pillar at different widths ranging from narrow to wide size is needed

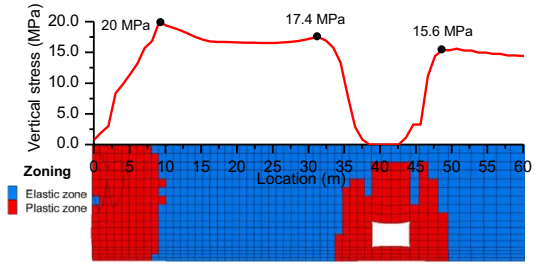

(a) Stage I) Panel8104 at the measurment station

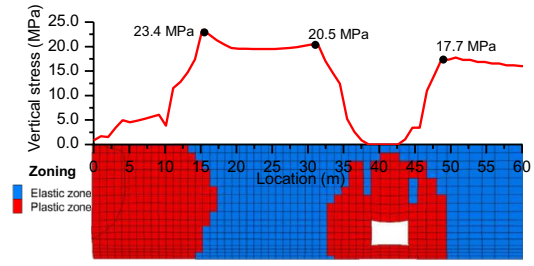

(b) Stage I) Panel8104 50m beyond the measurment station

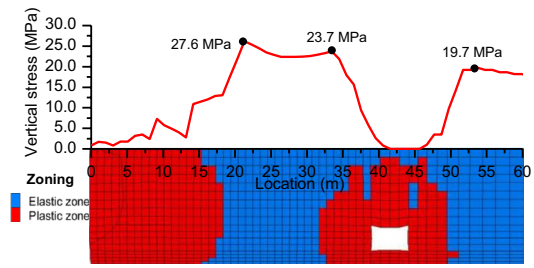

(c) Stage I) Panel8104 100m beyond the measurment station

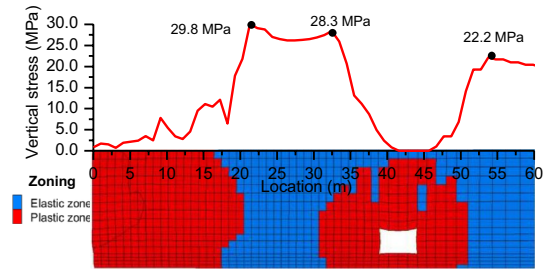

(d) Stage I) Panel8104 200m beyond the measurment station

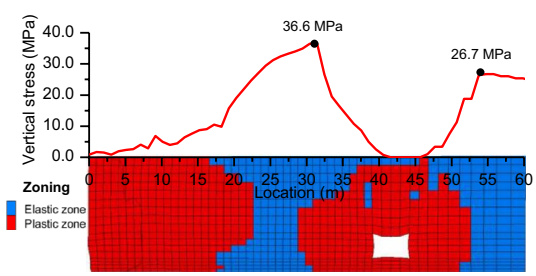

(e) Stage II) Panel8103 100m ahead of measurment station

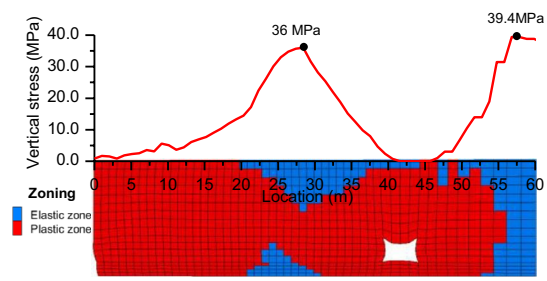

(f) Stage II) Panel8103 50m ahead of measurment station

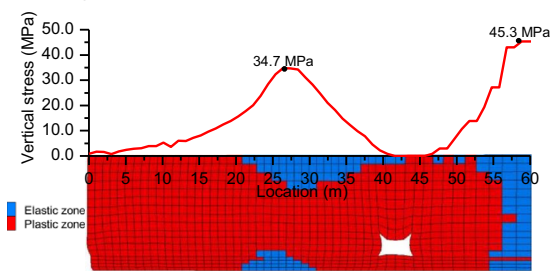

(g) Stage II) Panel8103 30m ahead of measurment station

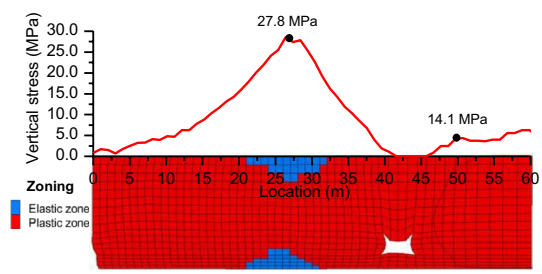

(h) Stage II) Panel8103 10m ahead of measurment station

Fig. 13 Numerical predictions of vertical stress profiles above the long gateroad pillar during the retreat of panels8104 (stage I) and 8103 (stage II)

which can only be undertaken using the numerical modelling. The developed numerical model in Fig. 11 is used for such a practice to estimate the stress profile on the pillars with various widths.

It is noteworthy that while wider pillars are desirable due to their high strength and better stability condition, their application can potentially lead to substantial coal loss. Therefore, a rigorous sensitivity

Table 10 Simulation results of the long gateroad pillar during the retreat of panels8104 (stage I) and 8103 (stage II)

	Mining stage	Maximum vertical stress (MPa)		Elastic zone in pillar(m)
		pillar	block side	
Panel 8104	At the measurment station	20 (Goaf side) 17.4 (Tailgate side)	15.6	23
	50 m beyond the measurment	23.4 (Goaf side) 20.5 (Tailgate side)	17.7	15
	100 m beyond the measurment	27.6 (Goaf side) 23.7 (Tailgate side)	19.7	13
	200 m beyond the measurment	29.8 (Goaf side) 28.3 (Tailgate side)	22.2	10
Panel 8103	100 m ahead of measurment station	36.6	26.7	6
	50 m ahead of measurment station	36	39.4	0
	30 m ahead of measurment station	34.7	45.3	0
	10 m ahead of measurment station	27.8	14.1	0

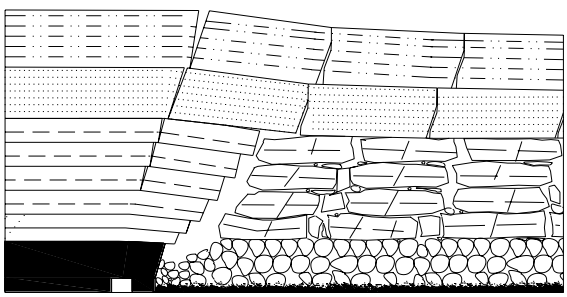

Fig. 14 Roof collapse pattern after one side is mined out with narrow long gateroad pillar

analysis is needed which should include a range of pillar widths from narrow size (e.g. less than 15 m) to a wide size (e.g. beyond 30 m). The earlier longwall coal mining practices in China demonstrated that the use of narrow pillars with the widths ranging from 4 to 15 m can be feasible (Wang et al. 2022; He et al. 2021a, b). However, none of the past operations were in the extra-thick coal seam under strong roof condition such as the case in Tongxin coal mine.

Typically, in the extra-thick coal seam longwall retreat, it is expected to observe a high caving zone particularly due to the presence of strong sand stone roof. Such a competent roof condition can cause formation of a very long cantilever beam before its failure during the retreat (see Fig. 14). When the roof fails, a large-scale cantilever beam tends to bend with the long gateroad pillar as the pivot, resulting in a generation of an extensive additional load on the pillar. The narrow long gateroad pillar is very susceptible to such an excessive load which can then lead to its failure. Therefore, it can be hypothesised that a wider pillar under such a roof condition due to its higher load carrying capacity can stay stable. However, the optimum width of such a wide pillar is an important issue for maximum coal recovery. As a result, to address this issue initially four different wide pillars with 38, 45, 50 and 55 m are considered for the sensitivity analysis followed by additional investigation of a narrow pillar having 8 m width. These widths are within the reasonable range that are commonly utilized in Chinese underground coal mines. The vertical stress profile and the potential yielding zone at different pillar widths are modelled based on the same panels extraction sequence that was utilized in practice where panel8104 was retreated first (stage I) followed by panel8103 (stage II).

Figure 15 summarises the modelling results obtained from the long gateroad pillars with various widths. It shows the plan view of yielded zones and the vertical stress profile at 1.8 m above the gateroad floor level. The results include both stages (I and II) of panels extraction. It is noteworthy that the numerical results of only 120 m length of long gateroad pillar are presented here. Such a length is selected based on a typical underground longwall mining practice where a pillar from the "chain pillars" can have a length up to 120 m. For stage I, the complete extraction of panel8104 is included while for stage II, the extraction of panel8103 at mid-point of the selected 120 m length of long gateroad is considered.

From Fig. 15 the increase in the induced vertical stress on the pillars is evident where only one panel (8104) is retreated versus both panels (8104 and 8103). Also, greater yield zone is estimated for the stage II of operation. It is clear that the pillars with

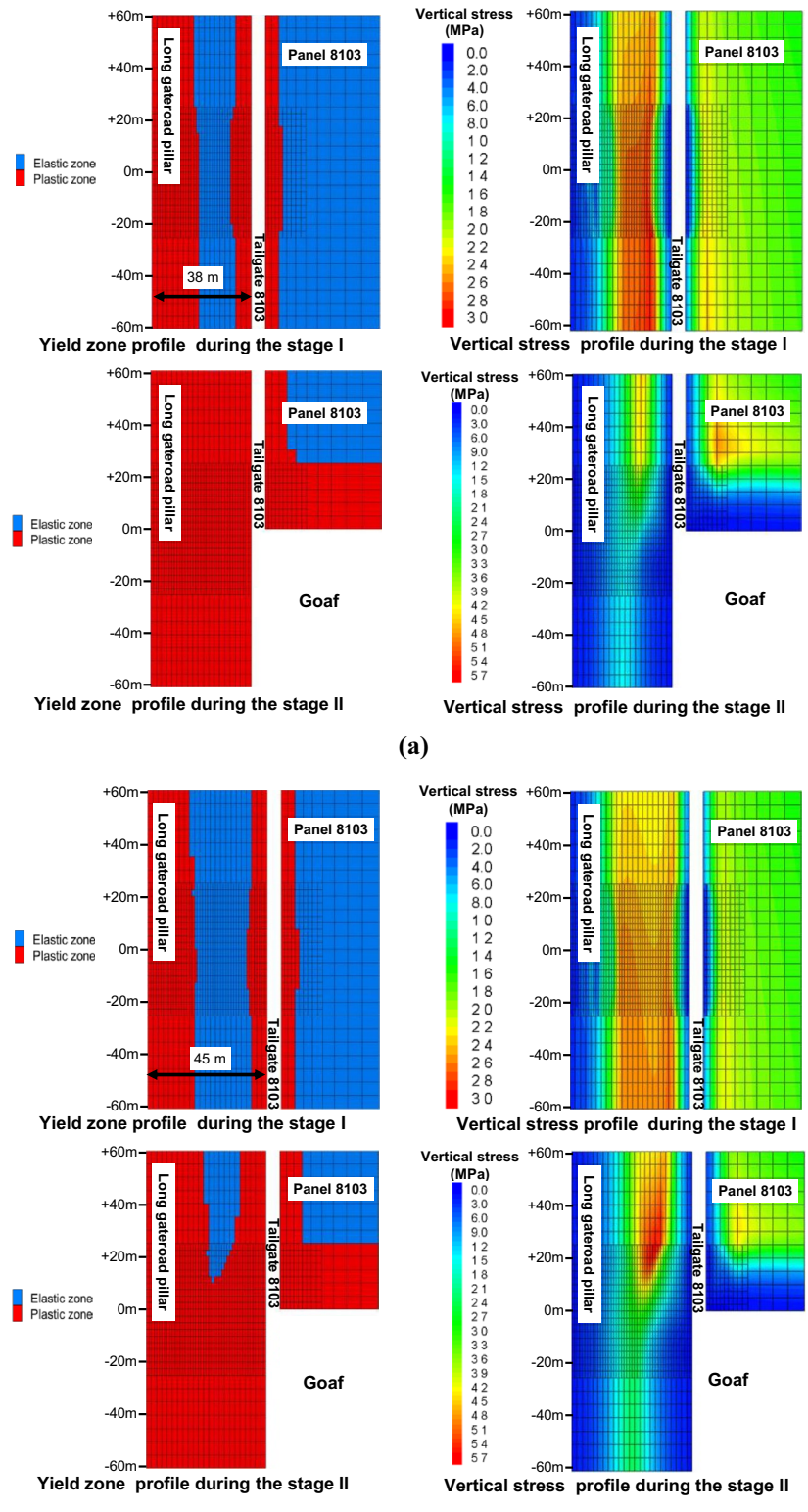

Fig. 15 Plan view of the numerical results obtained from the simulations of long gateroad pillars with **a** 38 m, **b** 45 m, **c** 50 m and **d** 55 m width

Fig. 15 (continued)

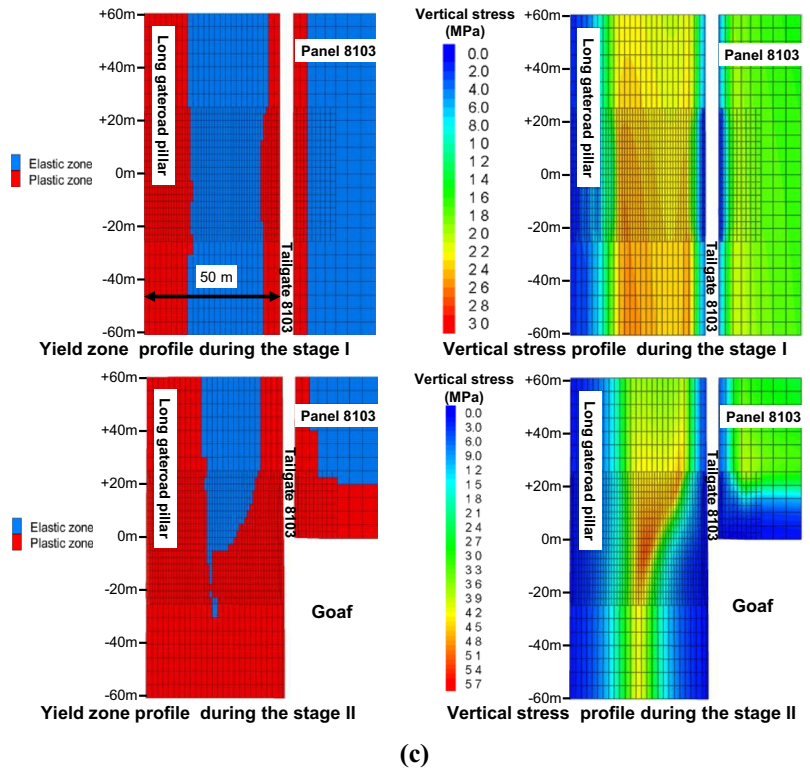

(c)

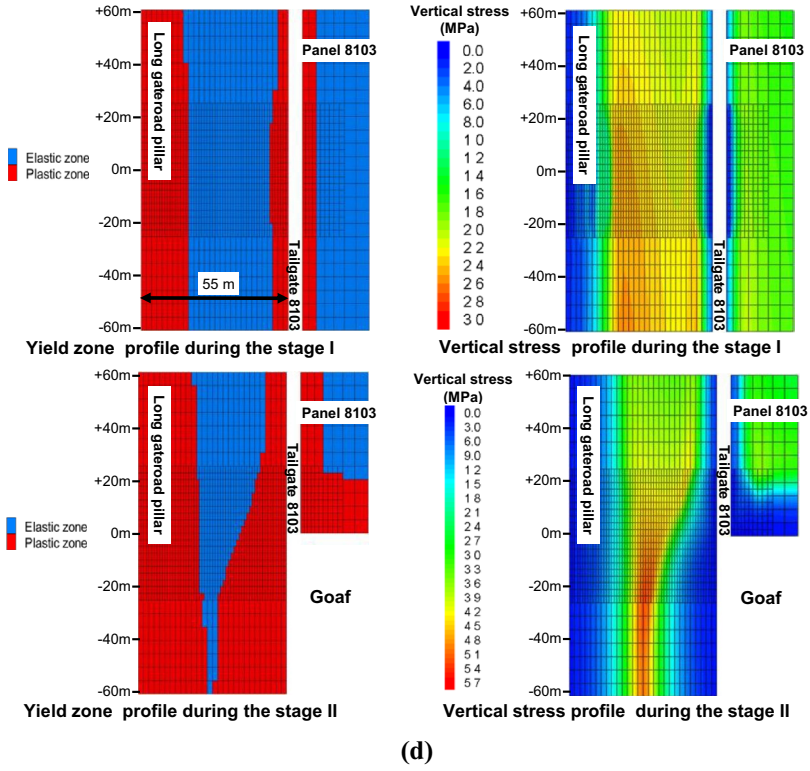

(d)

the greater widths can hold further induced vertical stress leading to a reduction in the yield zone.

During the stage I of modelling (extraction of panel8104), 18 m wide yield zone at the goaf side of pillar remains unchanged for all four widths while, the predicted yield zone on the tailgate side is different. For 38 and 45 m wide pillars, the yield zone on the gateroad side is approximately 8 m (Fig. 15a, b) whereas for the wider pillars (50 and 50 m), it is about 7 m (Figs. 15c-d). The vertical stress profile for wider pillars are at the lower range compared to the pillars with the smaller width. The centre part of pillar with elastic deformation increases from 26% in 38 m wide pillar to about 54% in the pillar with 55 m width.

During the stage II of modelling (extraction of panel8103), the performance of long gateroad pillars with various widths are compared when the panel8103 is at the centre point of 120 m selected length of pillar (see Fig. 15a–d). In particular, the behaviour of pillar at 60 m ahead of the longwall face (1), adjacent to the face (2) and 60 m behind the longwall face is analysed. For case (1), the long gateroad pillar with 38 m width was predicted to yield completely while the minimum yield zone was predicted for the pillar with 55 m width. The maximum induced vertical stress on the pillar with 38 m width is about 42 MPa while other pillars can carry higher vertical stresses. Adjacent to the longwall face (2), both 38 m and 45 m wide long gateroad pillars are predicted to yield completely whereas pillars with 50 and 55 m width can carry some load under elastic deformation. At this point, the maximum induced vertical stress on the smallest pillar is estimated to be about 20 MPa while such a stress is predicted to be approximately 55 MPa in the pillars with 50 and 55 m widths. Finally, the pillars behaviour at 60 m behind the longwall face (3) found to be consistent with those with 38, 45 and 50 m width exhibiting complete yielding. Only the 55 m wide pillar left with a small area under the elastic loading deformation. At this point, the smallest pillar is predicted to carry about 12 MPa vertical stress while the pillar with 45 m width is estimated to take three times higher vertical stress than the smallest pillar, at about 33 MPa. The induced vertical stress on the widest pillar is about 57 MPa whereas the second widest pillar is predicted to carry about 42 MPa vertical stress at 60 m behind the longwall face of panel 8103.

From the above analysis, it is clear that both 50 and 55 m wide pillars can be the ideal widths for the future longwall panels to ensure the maximum safety. Thus, to improve the coal recovery, the utilisation of 50 m wide pillar is recommended.

During the face retreat of panel8103, the extensive overhang roof in the goaf area can lead to an increase in the abutment stress on the long gateroad pillar. If a narrow long gateroad pillar having 8 m width is adopted, the whole pillar fails (see Fig. 16) along with the significant deformation of adjacent roadway as demonstrated in Fig. 17. This highlights the competency and advantage of wide long gateroad pillars which can always have an intact portion to bear the loading from the roof.

Ventilation and spontaneous combustion issues are also inevitable when small long gateroad pillar was used. In this case study, the coal seam is gassy and it is expected the goaf area in the previous panel has substantial methane concentration. As such, the methane is very likely to breathe into the tailgate of the current longwall panel especially when the small long gateroad pillar has induced fractures leading to an increase in its permeability for gas. On the other hand, the fresh air from the current tailgate is also likely to breathe out to the goaf area in the previous panel. These gas flow between panels would lead to the mixing of oxygen and methane, which would eventually increase the risk of spontaneous combustion. By contrast, a wide long gateroad pillar, which has at least some intact portion even under the abutment pressure, could minimise the methane breathe in and air breathe out issues considering its intrinsic lower permeability characteristics. As such, the wide long gateroad pillar has its distinguished advantage over the small long gateroad pillar for minimising the spontaneous combustion risks in this case study.

5 Discussions

5.1 Deep roof blasting of goaf edge to improve mining conditions

Overhanging competent roof on the goaf side induce a huge load on pillars and large deformations in surrounding strata. The pre-blasting measures can be used to minimise hanging roof spans and hence reduce the load transferred to the coal pillar.

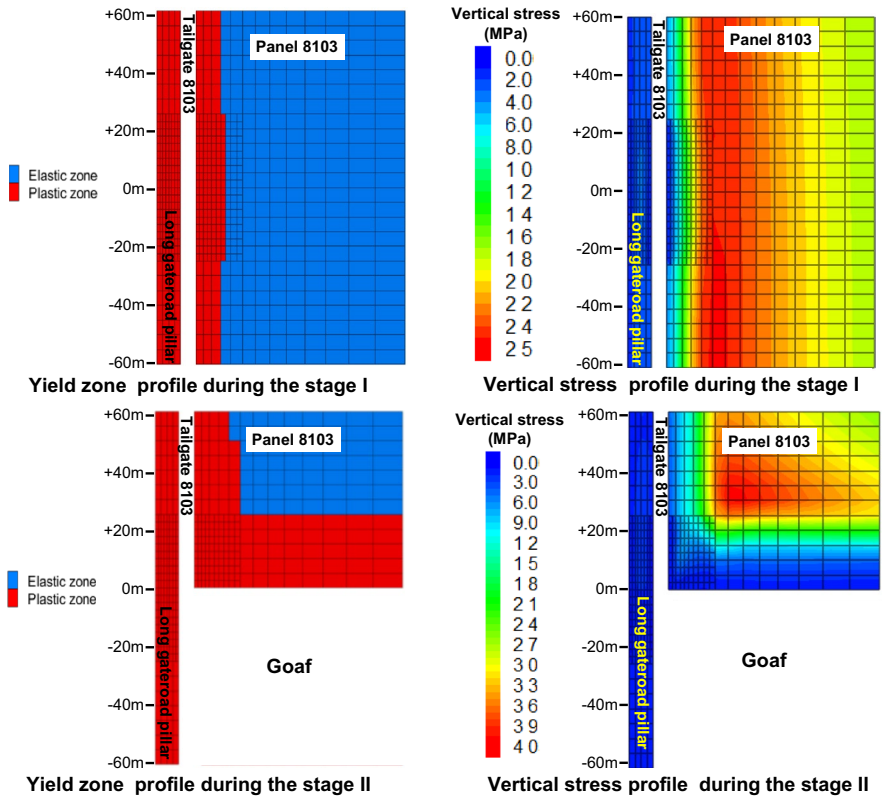

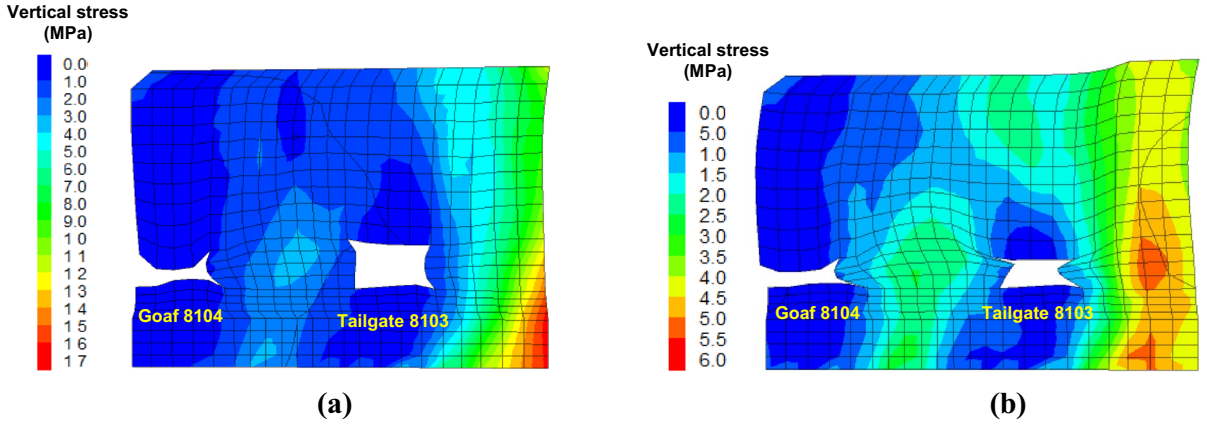

Fig.16 Plan view of the numerical results obtained from the simulations of long gateroad pillars having 8 m width

Fig.17 Behaviour of 8 m pillar under simulated loading: **a** cross-section of pillar and tailgate8103 after retreat of panel8104 and **b** cross-section of pillar and tailgate8103 at 10 m ahead of panel8103 face

Blasting adjacent to the caving zone was trialled in the model to show how stress relief can be achieved within the mining area. Blasting in the competent roof 80 m above the tailgate was chosen to be consistent with the competent roof caving height measured by other researchers in the Tongxin mine. Coal pillars 38 m, 45 m and 50 m wide were modelled with and without of the influence blasted roof. Stress distribution and strata yielding characteristics 10 m ahead of the 8103 longwall face were analysed and compared in Fig. 18 and Table 11.

In 38 m wide pillar, the extensive plastic zones and stress distributions were modelled, indicating entire pillar fails regardless of pre-blasting or not. When widening the pillar to 45 m, the pre-blasting measures could result in forming a 5 m wide elastic section in the centre of the pillar while the peak vertical stress was reduced from 60 to 53 MPa. For 50 m wide pillar, the elastic core zone was further increased to 9 m if no pre-blasting and 14 m if pre-blasting whereas vertical stress was reduced to 56 MPa and 41 MPa, respectively. In terms of the roadway closure, 38 m wide pillar led to a 1910 mm and 1516 mm horizontal convergence subjected to no pre-blasting and pre-blasting conditions, respectively. By contrast, the horizontal convergence for 45 mm wide pillar are 1688 mm and 1260 mm whereas that for the 50 m wide pillar are 1181 mm and 890 mm. In addition, the vertical convergence for 38 m wide pillar under no pre-blasting and pre-blasting conditions are 2050 mm and 1577 mm, respectively while that for 45 mm wide pillars are 1827 mm and 1314 mm, and that for 50 m wide pillars are 1327 mm and 992 mm, respectively. As such, it indicates that pillars more than 45 m wide could provide a sufficient ground support (Table 11).

5.2 Strengths of this study

The numerical model simulating the rock and coal in layers based on the strain-softening ubiquitous-joint constitutive model in FLAC^{3D} is more realistic as it includes discontinuities and intact rocks in the model. As such, the proposed model is capable of simulating different types of failures in intact rock and/or discontinuities during the mining operation. Either failure might lead to collapse in roof or sidewall. It is noteworthy that the discrete element modelling methodology by various numerical software (e.g. PFC, UDEC and 3DEC) is also capable of simulating discontinuities but the limitations are their significant computing time and excessive number of input parameters that are different to determine. Considering the scale of the model in this study, it is decided to employ FLAC^{3D} for simulating and numerical calculations.

In addition, a real case study in Tongxin coal mine has been conducted to validate the proposed numerical model indicating the capability and reliability of the model for predicting the rock behaviour in the underground mine of interest. The validated model can be potentially further utilised for a comprehensive sensitivity analysis to systematically analyse the ground stability and hence improve the ground support design.

5.3 Limitations of this study

For the simplicity of the modelling process, the coal and rock at the longwall face have been modelled as a continuum medium whereas in reality, the rock in the roof is more likely a discontinuum due to the fractures induced by the mining operations. Such a simplification might not 100% reflect the field conditions but it can significantly reduce the modelling complexities without adversely compromising the quality of the modelling results.

In addition, the failure mechanism under the dynamic loading condition has not been captured in this study. This might be especially more important when a competent roof is present as the longwall face advances, the collapse of the competent roof might delay leading to a significantly accumulation of the length of hanging roof. Thus, when the hanging roof collapses, a huge dynamic load would be induced that might result in the failures in the surrounding rock as well as longwall face.

6 Conclusions

A case study on pillar stability in Tongxin coal mine in China was performed. With the aid of borescope, the extent of damage within the long gateroad pillar during the extraction of both panels was quantified.

A numerical model were developed within the finite difference framework using FLAC^{3D} for a longwall panel in Tongxin coal mine in China. The geotechnical core logging data was utilized for the numerical models' development and calibration. The numerical results were compared with an analytical model proposed by (Salamon 1990) for validation followed by the vertical stress profile estimation of the long gateroad pillar under various panels extraction stages.

Finally, an extensive sensitivity analysis, comparing the wide and small long gateraod pillars, was performed to assess the optimum width of the long gateroad pillar for the future panels. It was concluded that the 50 m wide long gateroad pillar was an ideal size based on the geotechnical considerations.

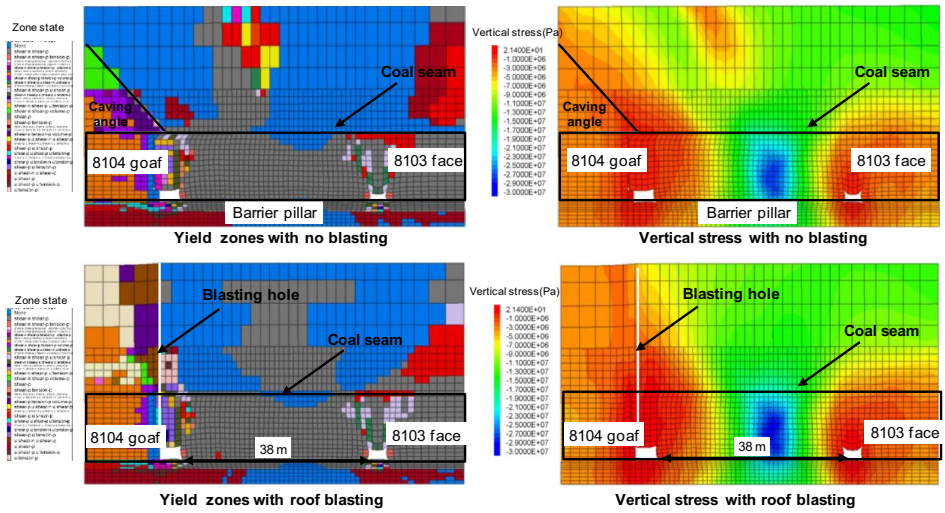

(a) Cross-section of 38 m coal pillar 10 m ahead of 8103 face (Stage II)

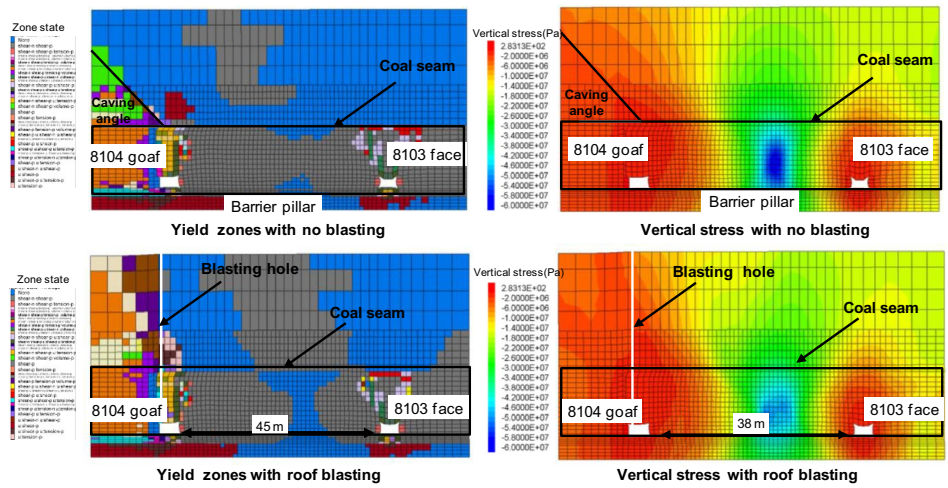

(b) Cross-section of 45m coal pillar10 m ahead of 8103 face (Stage II)

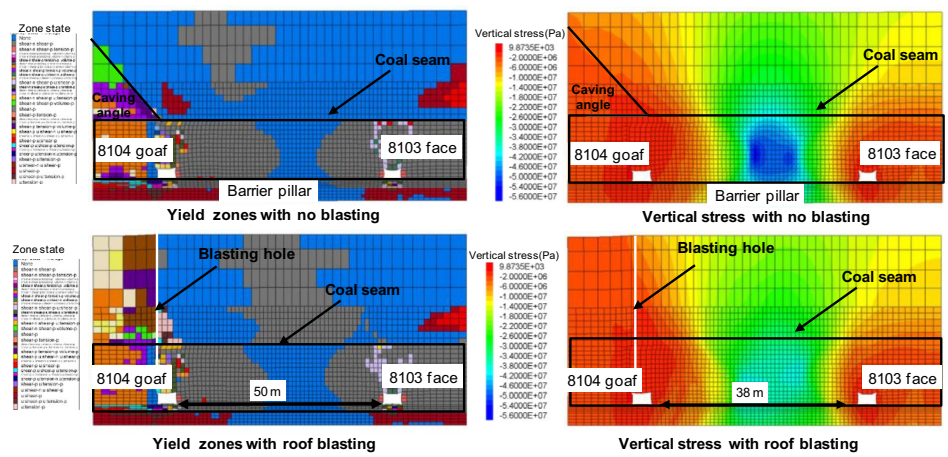

(c) Cross-section of 50m coal pillar10 m ahead of 8103 face (Stage II)

Fig.18 Stress and failure comparison for various pillar sizes with roof blasting and no blasting

Table 11 Summary of strata conditions roof blasting and no blasting for different pillar sizes

Pillar width (m)	Case	Horizontal convergence (mm)	Vertical convergence (mm)	Width of elastic core zone (m)	Peak vertical stress in pillar (MPa)
38	No blasting	1910	2050	0	27.8
	Roof blasting	1516	1577	0	29.7
45	No blasting	1688	1827	0	60
	Roof blasting	1260	1314	5	53.1
50	No blasting	1181	1327	9	56
	Roof blasting	890	992	14	41

Acknowledgements This work was supported by State Key Laboratory of Coal Mining and Clean Utilization(2021-CMCU-KF016) and Basic Scientific Research Projects of Universities in Liaoning Province(LJKZ0343).

Funding Open Access funding enabled and organized by CAUL and its Member Institutions.

Declarations

Conflict of interests On behalf of all authors, the corresponding author states that there is no conflict of interest.

References

Bai Q, Tu S, Wang F, Zhang C (2017) Field and numerical investigations of gateroad system failure induced by hard roofs in a longwall top coal caving face. Int J Coal Geol 173:176–199

Barron K (1984) An analytical approach to the design of coal pillars. CIM Bull 77(868):37–44

Bieniawski Z (1968) The effect of specimen size on compressive strength of coal. Int J Rock Mech Min Sci Geomech Abstr 5(4):325–335

Chen Y, Zhang HW, Yu B, Zhu ZJ, Wu WD, Li YP (2016) Study of influence of regional geodynamic background on strata behaviors in China's Tongxin mine. Resour Geol 66(1):1–11

Coggan J, Gao FQ, Stead D, Elmo D (2012) Numerical modelling of the effects of weak immediate roof lithology on coal mine roadway stability. Int J Coal Geol 90:100–109

Das AJ, Mandal PK, Bhattacharjee R, Tiwari S, Kushwaha A, Roy LB (2017) Evaluation of stability of underground workings for exploitation of an inclined coal seam by the ubiquitous joint model. Int J Rock Mech Min Sci 93:101–114

Das AJ, Mandal PK, Paul PS, Sinha RK, Tewari S (2019) Assessment of the strength of inclined coal pillars through numerical modelling based on the ubiquitous joint model. Rock Mech Rock Eng 52(10):3691–3717

Deng J, Kanwar NS, Pandey MD, Xie WC (2019) Dynamic buckling mechanism of pillar rockbursts induced by stress waves. J Rock Mech Geotech Eng 11(5):944–953

Roberts DP, Van der Merwe JN, Canbulat I, Sellers EJ, Coetzer S (2002). Development of a method to estimate coal pillar loading. Safety in Mines Research Advisory Committee Report

Forbes B, Vlachopoulos N, Diederichs MS, Hyett AJ, Punkkinen A (2020) An in situ monitoring campaign of a hard rock pillar at great depth within a Canadian mine. J Rock Mech Geotech Eng 12(3):427–448

Galvin J (2016) Ground engineering-principles and practices for underground coal mining. Springer, Cham

Galvin J, Hebblewhite B (1995) UNSW pillar design procedure. Strata Control for Coal Mine Design, The University of New South Wales

Ghasemi E, Shahriar K (2012) A new coal pillars design method in order to enhance safety of the retreat mining in room and pillar mines. Saf Sci 50(3):579–585

He M, Wang Q, Wu Q (2021a) Innovation and future of mining rock mechanics. J Rock Mech Geotech Eng 13(1):1–21

He Q, Zhu L, Li Y, Li D, Zhang B (2021b) Simulating hydraulic fracture re-orientation in heterogeneous rocks with an improved discrete element method. Rock Mech Rock Eng 54(6):2859–2879

Hill D (2005). Coal pillar design criteria for surface protection. In: 6th Australasian Coal Operators' Conference. pp 31–37

Hu SC, Tan YL, Zhou H, Ru WK, Ning JG, Wang J, Huang DM, Li Z (2019) Anisotropic modeling of layered rocks

incorporating planes of weakness and volumetric stress. Energy Sci Eng
Hustrulid W (1976) A review of coal pillar strength formulas. Rock Mech 8(2):115–145
Itasca F (2011) FLAC-Fast lagrangian analysis of continua, Version .7.0. Itasca Consulting Group Inc., Minneapolis
Jaiswal A, Shrivastva BK (2009) Numerical simulation of coal pillar strength. Int J Rock Mech Min Sci 46(4):779–788
Jiang L, Zhang P, Chen L, Hao Z, Sainoki A, Mitri HS, Wang Q (2017) Numerical approach for goaf-side entry layout and yield pillar design in fractured ground conditions. Rock Mech Rock Eng 50(11):3049–3071
Li W, Bai J, Peng S, Wang X, Xu Y (2014) Numerical modeling for yield pillar design: a case study. Rock Mech Rock Eng 48(1):305–318
Li D, Cai M, Masoumi H (2021) A constitutive model for modified cable bolts exhibiting cone shaped failure mode. Int J Rock Mechanics and Mining Sciences 145:104855
Li D, Li Y, Chen J, Masoumi H (2021) An analytical model for axial performance of rock bolts under constant confining pressure based on continuously yielding criterion. Tunn Undergr Space Technol 113:103955
Lorig L, Cabrera A (2013) Pillar strength estimates for foliated and inclined pillars in schistose material. In: Proceedings of the 3rd International FLAC/DEM Symposium, Hangzhou, China
Mark C, Chase FE, Campoli AA (1995) Analysis of retreat mining pillar stability. West Virginia Univ, Morgantown
Masoumi H, Bahaaddini M, Kim G, Hagan P (2014). Experimental investigation into the mechanical behavior of gosford sandstone at different sizes. In: 48th U.S. Rock Mechanics/Geomechanics Symposium
Masoumi H, Saydam S, Hagan PC (2016) Unified size-effect law for intact rock. Int J Geomech 16(2):04015059
Masoumi H, Roshan H, Hagan PC (2017) Size-dependent hoek-brown failure criterion. Int J Geomech 17(2):04016048
Masoumi H, Roshan H, Hedayat A, Hagan PC (2018) Scale-size dependency of intact rock under point-load and indirect tensile Brazilian testing. Int J Geomech 18(3):04018006
Mo S, Ramandi HL, Oh J, Masoumi H, Canbulat I, Hebblewhite B, Saydam S (2020) A new coal mine floor rating system and its application to assess the potential of floor heave. Int J Rock Mech Min Sci 128:104241
Mohan GM, Sheorey PR, Kushwaha A (2001) Numerical estimation of pillar strength in coal mines. Int J Rock Mech Min Sci 38(8):1185–1192
Peng SS (2019) Longwall mining. CRC Press, London
Prassetyo SH, Irnawan MA, Simangunsong GM, Wattimena RK, Arif I, Rai MA (2019) New coal pillar strength formulae considering the effect of interface friction. Int J Rock Mech Min Sci 123:104102
Recio-Gordo D, Jimenez R (2012) A probabilistic extension to the empirical ALPS and ARMPS systems for coal pillar design. Int J Rock Mech Min Sci 52:181–187
Reed G, McTyer K, Frith R (2017) An assessment of coal pillar system stability criteria based on a mechanistic evaluation of the interaction between coal pillars and the overburden. Int J Min Sci Technol 27(1):9–15
Sainsbury B, Pierce M, Mas Ivars D (2008) Simulation of rock mass strength anisotropy and scale effects using a Ubiquitous Joint Rock Mass (UJRM) model. In: Proceedings first international FLAC/DEM symposium on numerical modelling
Sainsbury BL, Sainsbury DP (2017) Practical use of the ubiquitous-joint constitutive model for the simulation of anisotropic rock masses. Rock Mech Rock Eng 50(6):1507–1528
Salamon MDG (1970) Stability, instability and design of pillar workings. Int J Rock Mech Min Sci Geomech Abstr 7(6):613–631
Salamon MDG, Munro AH (1967) A study of strength of coal pillars. J S Afr Inst Min Metall 68(2):55–000
Salamon MDG, Ozbay MU, Madden BJ (1998) Life and design of bord-and-pillar workings affected by pillar scaling. J S Afr Inst Min Metall 98(3):135–145
Salamon M (1990) Mechanism of caving in longwall coal mining. Rock mechanics contributions and challenges. In: Proceedings of the 31st US Symposium, Golden, Colorado
Shaojie C, Hailong W, Huaiyuan W, Weijia G, Xiushan L (2016) Strip coal pillar design based on estimated surface subsidence in eastern China. Rock Mech Rock Eng 49(9):3829–3838
Sheorey P, Singh TN, Singh B (1981) Considerations for the stability of longwall chain pillars and adjacent roadway. Dev Geotech Eng 32:129–133
Singh GSP, Singh UK (2009) A numerical modeling approach for assessment of progressive caving of strata and performance of hydraulic powered support in longwall workings. Comput Geotech 36(7):1142–1156
Sinha S, Walton G (2019) Numerical analyses of pillar behavior with variation in yield criterion, dilatancy, rock heterogeneity and length to width ratio. J Rock Mech Geotech Eng 11(1):46–60
Sinha S, Walton G (2020) Modeling behaviors of a coal pillar rib using the progressive S-shaped yield criterion. J Rock Mech Geotech Eng 12(3):484–492
Vardar O, Zhang C, Canbulat I, Hebblewhite B (2019) Numerical modelling of strength and energy release characteristics of pillar-scale coal mass. J Rock Mech Geotech Eng 11(5):935–943
Wang Y, Li YM, Yu ZL, Zhang H, Ding D (2022) Research on the surrounding rock control technology of gob-side entry with a narrow coal pillar reserved in a fully mechanized caving face with large mining height. Geotech Geol Eng 40:285–300
Whittaker BN, Singh RN (1981) Stability of Longwall mining gate roadways in relation to rib pillar size. Int J Rock Mech Min Sci Geomech Abstr 18(4):331–334
Wilson AH (1983) The stability of underground workings in the soft rocks of the coal measures. Int J Min Eng 1(2):91–187
Wu W-D, Bai J-B, Wang X-Y, Yan S, Wu S-X (2018) Numerical study of failure mechanisms and control techniques for a gob-side yield pillar in the Sijiazhuang coal mine, China. Rock Mech Rock Eng 52(4):1231–1245
Wu W-D, Bai J-B, Wang X-Y, Zhu Z-J, Yan S (2019) Field investigation of fractures evolution in overlying strata

caused by extraction of the jurassic and carboniferous coal seams and its application: case study. Int J Coal Geol 208:12–23

Zhai H, Masoumi H, Zoorabadi M, Canbulat I (2020) Size-dependent behaviour of weak intact rocks. Rock Mech Rock Eng 53(8):3563–3587

Zhang LY, Einstein HH (2004) Using RQD to estimate the deformation modulus of rock masses. Int J Rock Mech Min Sci 41(2):337–341

Zhang J, Jiang F, Zhu S, Zhang L (2016) Width design for gobs and isolated coal pillars based on overall burst-instability prevention in coal mines. J Rock Mech Geotech Eng 8(4):551–558

Zhang G-C, He F-L, Jia H-G, Lai Y-H (2017) Analysis of gateroad stability in relation to yield pillar size: a case study. Rock Mech Rock Eng 50(5):1263–1278

Zhu Z, Zhang H, Nemcik J, Lan T, Han J, Chen Y (2018) Overburden movement characteristics of top-coal caving mining in multi-seam areas. Q J Eng GeolHydrogeol 51(2):276–286

Zhu Z, Wu Y, Han J (2022) A prediction method of coal burst based on analytic hierarchy process and fuzzy comprehensive evaluation. Front Earth Sci. https://doi.org/10.3389/feart.2021.834958